CHAPTER 5

Walking

Practical legged locomotion is one of the fundamental unsolved problems in robotics. Many challenges are in mechanical design - a walking robot must carry all of it's actuators and power, making it difficult to carry ideal force/torque - controlled actuators. But many of the unsolved problems are because walking robots are underactuated control systems.

In this chapter we'll introduce some of the simple models of walking robots, the control problems that result, and a very brief summary of some of the control solutions described in the literature. Compared to the robots that we have studied so far, our investigations of legged locomotion will require additional tools for thinking about limit cycle dynamics and dealing with impacts.

5.1 LIMIT CYCLES

A limit cycle is an asymptotically stable or unstable periodic orbit[1]. One of the simplest models of limit cycle behavior is the Van der Pol oscillator. Let's examine that first...

EXAMPLE 5.1 Van der Pol Oscillator

$$\ddot{q} + \mu(q^2 - 1)\dot{q} + q = 0$$

One can think of this system as almost a simple spring-mass-damper system, except that it has nonlinear damping. In particular, the velocity term dissipates energy when $|q| > 1$, and adds energy when $|q| < 1$. Therefore, it is not terribly surprising to see that the system settles into a stable oscillation from almost any initial conditions (the exception is the state $q = 0, \dot{q} = 0$). This can be seem nicely in the phase portrait in Figure 5.1(left).

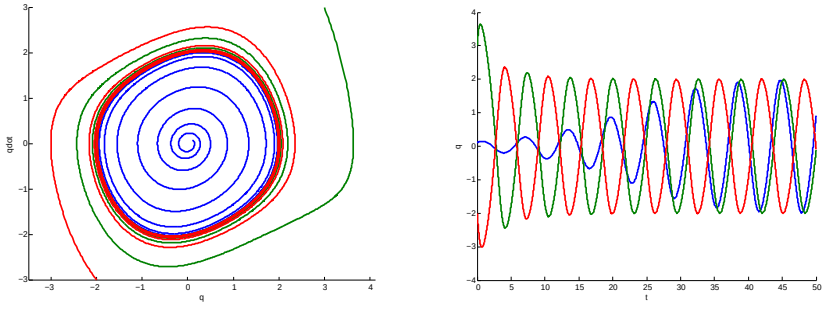

FIGURE 5.1 System trajectories of the Van der Pol oscillator with $\mu = .2$. (Left) phase portrait. (Right) time domain.

[1] marginally-stable orbits, such as the closed-orbits of the undamped simple pendulum, are typically not called limit cycles.

However, if we plot system trajectories in the time domain, then a slightly different picture emerges (see Figure 5.1(right)). Although the phase portrait clearly reveals that all trajectories converge to the same orbit, the time domain plot reveals that these trajectories do not necessarily synchronize in time.

The Van der Pol oscillator clearly demonstrates what we would think of as a stable limit cycle, but also exposes the subtlety in defining this limit cycle stability. Neighboring trajectories do not necessarily converge on a stable limit cycle. In contrast, defining the stability of a particular trajectory (parameterized by time) is relatively easy.

Let's make a few quick points about the existence of closed-orbits. If we can define a closed region of phase space which does not contain any fixed points, then it must contain a closed-orbit[83]. By closed, I mean that any trajectory which enters the region will stay in the region (this is the Poincare-Bendixson Theorem). It's also interesting to note that gradient potential fields (e.g. Lyapunov functions) cannot have a closed-orbit[83], and consquently Lyapunov analysis cannot be applied to limit cycle stability without some modification.

5.2 POINCARÉ MAPS

One definition for the stability of a limit cycle uses the method of Poincaré. Let's consider an n dimensional dynamical system, $\dot{\mathbf{x}} = \mathbf{f}(\mathbf{x})$. Define an $n-1$ dimensional *surface of section*, S. We will also require that S is tranverse to the flow (i.e., all trajectories starting on S flow through S, not parallel to it). The Poincaré map (or return map) is a mapping from S to itself:

$$\mathbf{x}_p[n+1] = \mathbf{P}(\mathbf{x}_p[n]),$$

where $\mathbf{x}_p[n]$ is the state of the system at the nth crossing of the surface of section. Note that we will use the notation $\mathbf{x}_p$ to distinguish the state of the discrete-time system from the continuous time system; they are related by $\mathbf{x}_p[n] = \mathbf{x}(t_c[n])$, where $t_c[n]$ is the time of the nth crossing of S.

EXAMPLE 5.2 Return map for the Van der Pol Oscillator

Since the full system is two dimensional, the return map dynamics are one dimensional. One dimensional maps, like one dimensional flows, are amenable to graphical analysis. To define a Poincare section for the Van der Pol oscillator, let S be the line segment where $\dot{q} = 0, q > 0$.

If $\mathbf{P}(\mathbf{x}_p)$ exists for all $\mathbf{x}_p$, then this method turns the stability analysis for a limit cycle into the stability analysis of a fixed point on a discrete map. In practice it is often difficult or impossible to find $\mathbf{P}$ analytically, but it can be obtained quite reasonably numerically. Once $\mathbf{P}$ is obtained, we can infer local limit cycle stability with an eigenvalue analysis. There will always be a single eigenvalue of 1 - corresponding to perturbations along the limit cycle which do not change the state of first return. The limit cycle is considered locally exponentially stable if all remaining eigenvalues, λ_i, have magnitude less than one, $|\lambda_i| < 1$.

In fact, it is often possible to infer more global stability properties of the return map by examining, $\mathbf{P}$. [44] describes some of the stability properties known for *unimodal* maps.

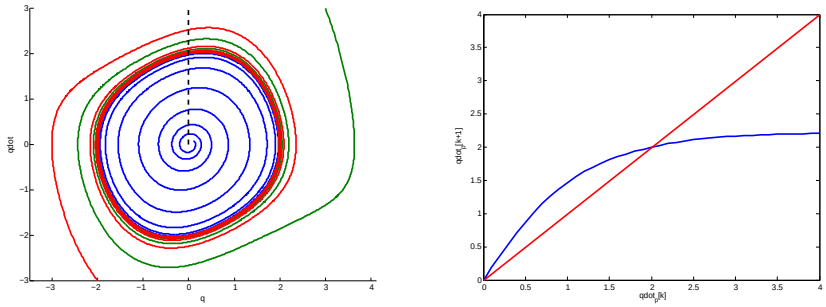

FIGURE 5.2 (Left) Phase plot with the surface of section, S drawn with a black dashed line. (Right) The resulting Poincare first-return map (blue), and the line of slope one (red).

A particularly graphical method for understanding the dynamics of a one-dimensional iterated map is with the staircase method. Sketch the Poincare map and also the line of slope one. Fixed points are the crossings with the unity line. Asymptotically stable if $|\lambda| < 1$. Unlike one dimensional flows, one dimensional maps can have oscillations (happens whenever $\lambda < 0$).

[insert staircase diagram of van der Pol oscillator return map here]

5.3 THE BALLISTIC WALKER

One of the earliest models of walking was proposed by McMahon[59], who argued that humans use a mostly ballistic (passive) gait. COM trajectory looks like a pendulum (roughly walking by vaulting). EMG activity in stance legs is high, but EMG in swing leg is very low, except for very beginning and end of swing. Proposed a three-link "ballistic walker" model, which models a single swing phase (but not transitions to the next swing nor stability). Interestingly, in recent years the field has developed a considerably deeper appreciation for the role of compliance during walking; simple walking-by-vaulting models are starting to fall out of favor.

McGeer[55] followed up with a series of walking machines, called "passive dynamic walkers". The walking machine by Collins and Ruina[26] is the most impressive passive walker to date.

5.4 THE RIMLESS WHEEL

The most elementary model of passive dynamic walking, first used in the context of walking by [55], is the rimless wheel. This simplified system has rigid legs and only a point mass at the hip as illustrated in Figure 5.3. To further simplify the analysis, we make the following modeling assumptions:

- Collisions with ground are inelastic and impulsive (only angular momentum is conserved around the point of collision).
- The stance foot acts as a pin joint and does not slip.
- The transfer of support at the time of contact is instantaneous (no double support phase).

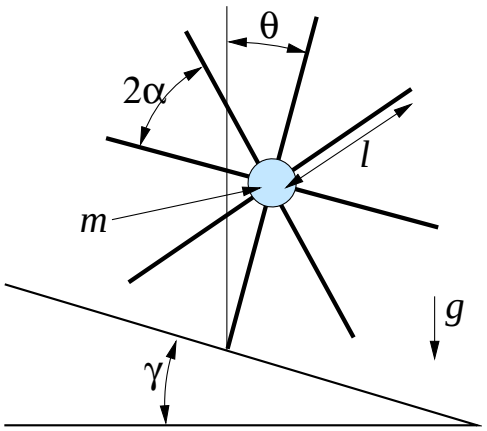

FIGURE 5.3 The rimless wheel. The orientation of the stance leg, θ, is measured clockwise from the vertical axis.

- $0 \leq \gamma < \frac{\pi}{2}, 0 < \alpha < \frac{\pi}{2}, l > 0.$

Note that the coordinate system used here is slightly different than for the simple pendulum ($\theta = 0$ is at the top, and the sign of θ has changed).

The most comprehensive analysis of the rimless wheel was done by [24].

5.4.1 Stance Dynamics

The dynamics of the system when one leg is on the ground are given by

$$\ddot{\theta} = \frac{g}{l} \sin(\theta).$$

If we assume that the system is started in a configuration directly after a transfer of support ($\theta(0^+) = \gamma - \alpha$), then forward walking occurs when the system has an initial velocity, $\dot{\theta}(0^+) > \omega_1$, where

$$\omega_1 = \sqrt{2\frac{g}{l}\left[1 - \cos\left(\gamma - \alpha\right)\right]}.$$

ω_1 is the threshold at which the system has enough kinetic energy to vault the mass over the stance leg and take a step. This threshold is zero for $\gamma = \alpha$ and does not exist for $\gamma > \alpha$. The next foot touches down when $\theta(t) = \gamma + \alpha$, at which point the conversion of potential energy into kinetic energy yields the velocity

$$\dot{\theta}(t^-) = \sqrt{\dot{\theta}^2(0^+) + 4\frac{g}{l}\sin\alpha\sin\gamma}.$$

t^- denotes the time immediately before the collision.

5.4.2 Foot Collision

The angular momentum around the point of collision at time t just before the next foot collides with the ground is

$$L(t^-) = -ml^2\dot{\theta}(t^-)\cos(2\alpha).$$

The angular momentum at the same point immediately after the collision is

$$L(t^+) = -ml^2\dot{\theta}(t^+).$$

Assuming angular momentum is conserved, this collision causes an instantaneous loss of velocity:

$$\dot{\theta}(t^+) = \dot{\theta}(t^-)\cos(2\alpha).$$

The deterministic dynamics of the rimless wheel produce a stable limit cycle solution with a continuous phase punctuated by a discrete collision, as shown in Figure 5.4. The red dot on this graph represents the initial conditions, and this limit cycle actually moves counter-clockwise in phase space because for this trial the velocities were always negative. The collision represents as instantaneous change of velocity, and a transfer of the coordinate system to the new point of contact.

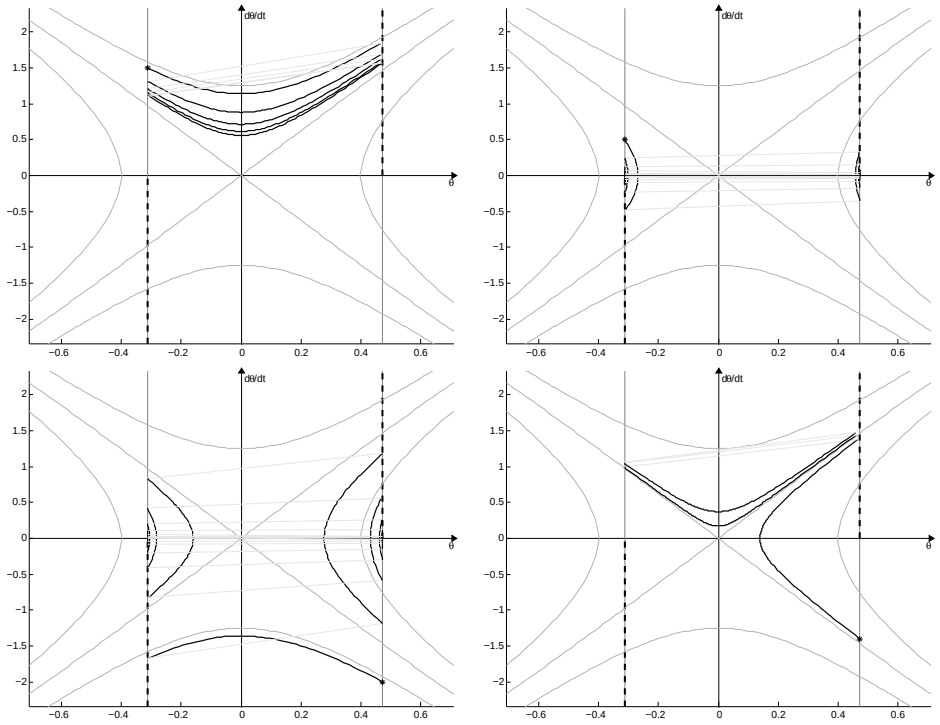

FIGURE 5.4 Phase portrait trajectories of the rimless wheel ($m = 1, l = 1, g = 9.8, \alpha = \pi/8, \gamma = 0.08$).

5.4.3 Return Map

We can now derive the angular velocity at the beginning of each stance phase as a function of the angular velocity of the previous stance phase. First, we will handle the case where $\gamma \leq \alpha$ and $\dot{\theta}_n^+ > \omega_1$. The "step-to-step return map", factoring losses from a single

collision, the resulting map is:

$$\dot{\theta}^+_{n+1} = \cos(2\alpha)\sqrt{(\dot{\theta}^+_n)^2 + 4\frac{g}{l}\sin\alpha\sin\gamma}.$$

where the $\dot{\theta}^+$ indicates the velocity just *after* the energy loss at impact has occurred.

Using the same analysis for the remaining cases, we can complete the return map. The threshold for taking a step in the opposite direction is

$$\omega_2 = -\sqrt{2\frac{g}{l}[1-\cos(\alpha+\gamma)]}.$$

For $\omega_2 < \dot{\theta}^+_n < \omega_1$, we have

$$\dot{\theta}^+_{n+1} = -\dot{\theta}^+_n\cos(2\alpha).$$

Finally, for $\dot{\theta}^+_n < \omega_2$, we have

$$\dot{\theta}^+_{n+1} = -\cos(2\alpha)\sqrt{(\dot{\theta}^+_n)^2 - 4\frac{g}{l}\sin\alpha\sin\gamma}.$$

Notice that the return map is undefined for $\dot{\theta}_n = \{\omega_1, \omega_2\}$, because from these configurations, the wheel will end up in the (unstable) equilibrium point where $\theta = 0$ and $\dot{\theta} = 0$, and will therefore never return to the map.

This return map blends smoothly into the case where $\gamma > \alpha$. In this regime,

$$\dot{\theta}^+_{n+1} = \begin{cases} \cos(2\alpha)\sqrt{(\dot{\theta}^+_n)^2 + 4\frac{g}{l}\sin\alpha\sin\gamma}, & 0 \le \dot{\theta}^+_n \\ -\dot{\theta}^+_n\cos(2\alpha), & \omega_2 < \dot{\theta}^+_n < 0 \\ -\cos(2\alpha)\sqrt{(\dot{\theta}^+_n)^2 - 4\frac{g}{l}\sin\alpha\sin\gamma}, & \dot{\theta}^+_n \le w_2 \end{cases}.$$

Notice that the formerly undefined points at $\{\omega_1, \omega_2\}$ are now well-defined transitions with $\omega_1 = 0$, because it is kinematically impossible to have the wheel statically balancing on a single leg.

5.4.4 Fixed Points and Stability

For a fixed point, we require that $\dot{\theta}^+_{n+1} = \dot{\theta}^+_n = \omega^*$. Our system has two possible fixed points, depending on the parameters:

$$\omega^*_{stand} = 0, \quad \omega^*_{roll} = \cot(2\alpha)\sqrt{4\frac{g}{l}\sin\alpha\sin\gamma}.$$

The limit cycle plotted in Figure 5.4 illustrates a state-space trajectory in the vicinity of the rolling fixed point. ω^*_{stand} is a fixed point whenever $\gamma < \alpha$. ω^*_{roll} is a fixed point whenever $\omega^*_{roll} > \omega_1$. It is interesting to view these bifurcations in terms of γ. For small γ, ω_{stand} is the only fixed point, because energy lost from collisions with the ground is not compensated for by gravity. As we increase γ, we obtain a stable rolling solution, where the collisions with the ground exactly balance the conversion of gravitational potential to kinetic energy. As we increase γ further to $\gamma > \alpha$, it becomes impossible for the center of mass of the wheel to be inside the support polygon, making standing an unstable configuration.

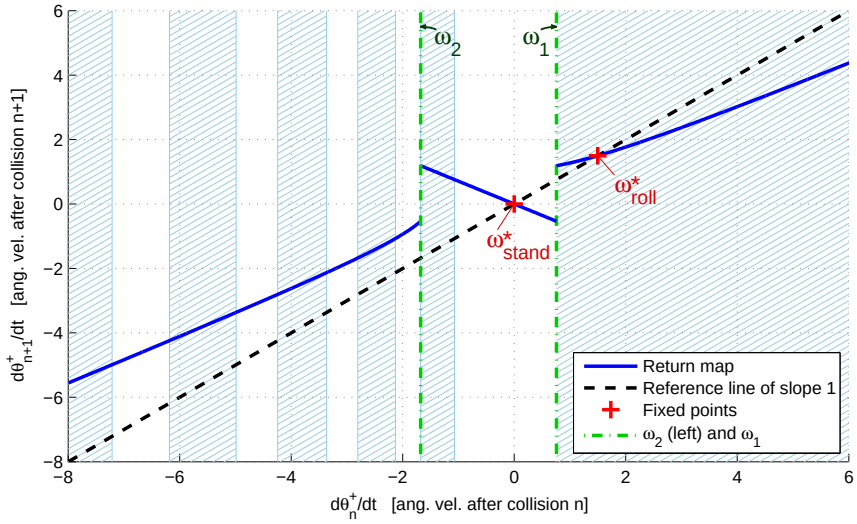

FIGURE 5.5 Limit cycle trajectory of the rimless wheel ($m = 1, l = 1, g = 9.8, \alpha = \pi/8, \gamma = 0.15$). All hatched regions converge to the rolling fixed point, ω^*_{roll}; the white regions converge to zero velocity (ω^*_{stand}).

5.5 THE COMPASS GAIT

The rimless wheel models only the dynamics of the stance leg, and simply assumes that there will always be a swing leg in position at the time of collision. To remove this assumption, we take away all but two of the spokes, and place a pin joint at the hip. To model the dynamics of swing, we add point masses to each of the legs. For actuation, we first consider the case where there is a torque source at the hip - resulting in swing dynamics equivalent to an Acrobot (although in a different coordinate frame).

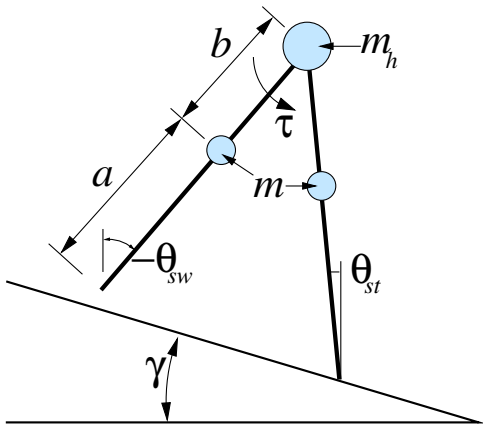

FIGURE 5.6 The compass gait

In addition to the modeling assumptions used for the rimless wheel, we also assume that the swing leg retracts in order to clear the ground without disturbing the position of the mass of that leg. This model, known as the compass gait, is well studied in the literature using numerical methods [36, 81], but relatively little is known about it analytically.

The state of this robot can be described by 4 variables: $\theta_{st}, \theta_{sw}, \dot{\theta}_{st}$, and $\dot{\theta}_{sw}$. The abbreviation st is shorthand for the stance leg and sw for the swing leg. Using $\mathbf{q} = [\theta_{sw}, \theta_{st}]^T$ and $\mathbf{u} = \tau$, we can write the dynamics as

$$\mathbf{H}(\mathbf{q})\ddot{\mathbf{q}} + \mathbf{C}(\mathbf{q}, \dot{\mathbf{q}})\dot{\mathbf{q}} + \mathbf{G}(\mathbf{q}) = \mathbf{B}\mathbf{u},$$

with

$$\mathbf{H} = \begin{bmatrix} mb^2 & -mlb\cos(\theta_{st} - \theta_{sw}) \\ -mlb\cos(\theta_{st} - \theta_{sw}) & (m_h + m)l^2 + ma^2 \end{bmatrix}$$
$$\mathbf{C} = \begin{bmatrix} 0 & mlb\sin(\theta_{st} - \theta_{sw})\dot{\theta}_{st} \\ mlb\sin(\theta_{st} - \theta_{sw})\dot{\theta}_{sw} & 0 \end{bmatrix}$$
$$\mathbf{G} = \begin{bmatrix} mbg\sin(\theta_{sw}) \\ -(m_h l + ma + ml)g\sin(\theta_{st}) \end{bmatrix},$$
$$\mathbf{B} = \begin{bmatrix} 1 \\ -1 \end{bmatrix}$$

and $l = a + b$. These equations come straight out of [37].

The foot collision is an instantaneous change of velocity governed by the conservation of angular momentum around the point of impact:

$$\mathbf{Q}^+(\alpha)\dot{\mathbf{q}}^+ = \mathbf{Q}^-(\alpha)\dot{\mathbf{q}}^-,$$

where

$$\mathbf{Q}^-(\alpha) = \begin{bmatrix} -mab & -mab + (m_h l^2 + 2mal)\cos(2\alpha) \\ 0 & -mab \end{bmatrix}$$
$$\mathbf{Q}^+(\alpha) = \begin{bmatrix} mb(b - l\cos(2\alpha)) & ml(l - b\cos(2\alpha) + ma^2 + m_h l^2 \\ mb^2 & -mbl\cos(2\alpha) \end{bmatrix}$$

and $\alpha = \frac{\theta_{sw} - \theta_{st}}{2}$.

Numerical integration of these equations reveals a stable limit cycle, plotted in Figure 5.7. The cycle is composed of a swing phase (top) and a stance phase (bottom), punctuated by two instantaneous changes in velocity which correspond to the ground collisions. The dependence of this limit cycle on the system parameters has been studied extensively in [37].

The basin of attraction of the stable limit cycle is a narrow band of states surrounding the steady state trajectory. Although the simplicity of this model makes it analytically attractive, this lack of stability makes it difficult to implement on a physical device.

5.6 THE KNEED WALKER

To achieve a more anthropomorphic gait, as well as to acquire better foot clearance and ability to walk on rough terrain, we want to model a walker that includes knee[41]. For this, we model each leg as two links with a point mass each.

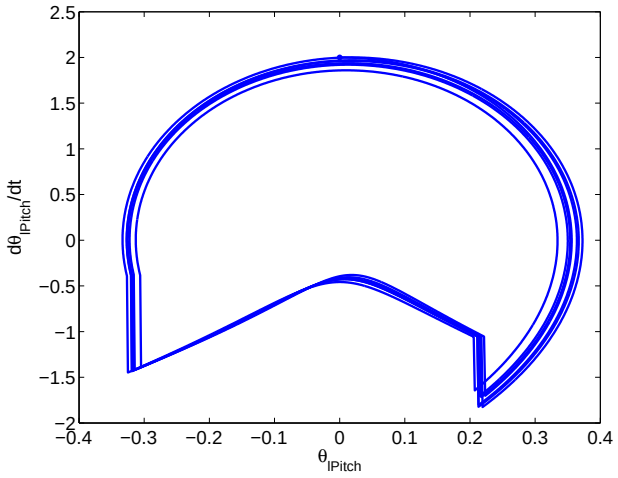

FIGURE 5.7 Limit cycle trajectory of the compass gait. ($m = 5$kg,$m_h = 10$kg,$a = b = 0.5$m,$\phi = 0.03$deg. $\mathbf{x}(0) = [0, 0, 2, -0.4]^T$). θ_{lPitch} is the pitch angle of the left leg, which is recovered from θ_{st} and θ_{sw} in the simulation with some simple book-keeping.

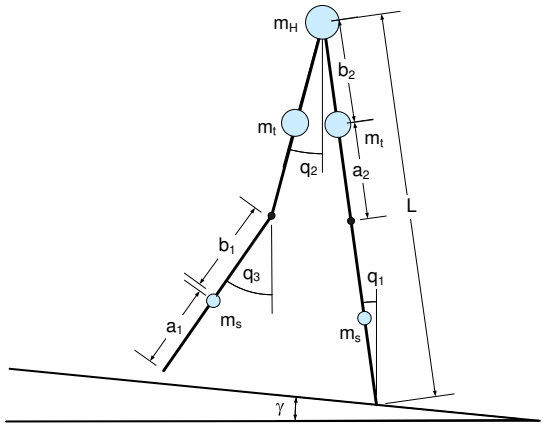

FIGURE 5.8 The Kneed Walker

At the beginning of each step, the system is modeled as a three-link pendulum, like the ballistic walker[59, 58, 81]. The stance leg is the one in front, and it is the first link of a pendulum, with two point masses. The swing leg has two links, with the joint between them unconstrained until knee-strike. Given appropriate mass distributions and initial conditions, the swing leg bends the knee and swings forward. When the swing leg straightens out (the lower and upper length are aligned), knee-strike occurs. The knee-strike is modeled as a discrete inelastic collision, conserving angular momentum and changing velocities instantaneously.

After this collision, the knee is locked and we switch to the compass gait model with a different mass distribution. In other words, the system becomes a two-link pendulum. Again, the heel-strike is modeled as an inelastic collision. After the collision, the legs switch instantaneously. After heel-strike then, we switch back to the ballistic walker's three-link pendulum dynamics. This describes a full step cycle of the kneed walker, which is shown in Figure 5.9.

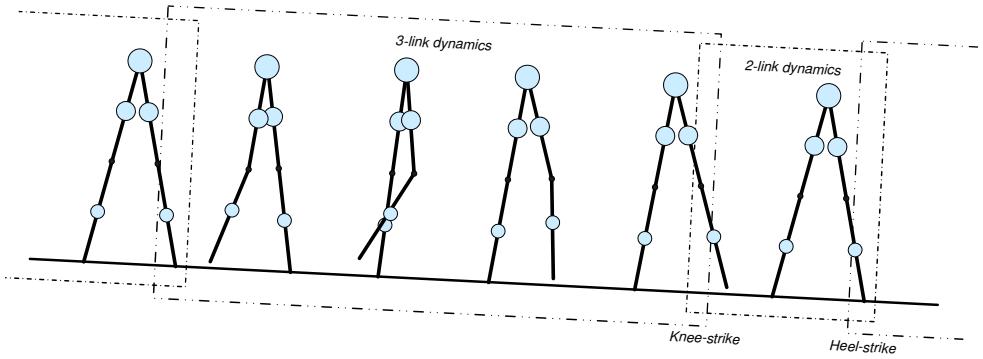

FIGURE 5.9 Limit cycle trajectory for kneed walker

By switching between the dynamics of the continuous three-link and two-link pendulums with the two discrete collision events, we characterize a full point-feed kneed walker walking cycle. After finding appropriate parameters for masses and link lengths, a stable gait is found. As with the compass gait's limit cycle, there is a swing phase (top) and a stance phase (bottom). In addition to the two heel-strikes, there are two more instantaneous velocity changes from the knee-strikes as marked in Figure 5.10. This limit cycle is traversed clockwise.

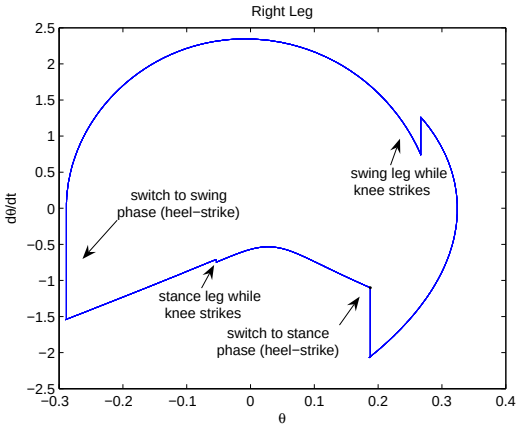

FIGURE 5.10 The Kneed Walker

5.7 NUMERICAL ANALYSIS

A note on integrating hybrid systems and/or evaluating return maps. The dynamics are often very sensitive to the switching plane. Often a good idea to back up integration to attempt to find collisions and transitions very accurately. MATLAB can handle this nicely with zero-crossings in the ODE solvers.

5.7.1 Finding Limit Cycles

You can find asymptotically stable limit cycles by integrating forward the ODE (until $t \rightarrow \infty$), as long as you can guess an initial condition inside the basin of attraction. This convergence rate will depend on the convergence rate around the fixed point and could be inefficient for complex systems, and guessing initial conditions is difficult for systems like the compass gait. This method won't work for finding unstable limit cycles.

Remember that a fixed point on the Poincare map:

$$\mathbf{x}_p[n+1] = \mathbf{P}(\mathbf{x}_p[n]),$$

is simply a zero-crossing of the (vector-valued) function

$$\mathbf{P}(\mathbf{x}_p[n]) - \mathbf{x}_p[n+1].$$

Therefore, an efficient way to obtain the fixed points numerically is to use an algorithm which finds the zero-crossings by a Newton method[16, 67][2]. These methods can be dramatically more efficient if one can efficiently estimate the gradient of the Poincare map.

Gradients of the Poincare map.
The Poincare map is defined by integrating the continuous dynamics,

$$\mathbf{x}(t_c^-[n+1]) = \mathbf{x}(t_c^+[n]) + \int_{t_c^+[n]}^{t_c^-[n+1]} \mathbf{f}(\mathbf{x}(t))dt, \quad \mathbf{x}(t_c^+[n]) = \mathbf{x}_p[n]$$

then applying the (discrete) impact dynamics

$$\mathbf{x}_p[n+1] = \mathbf{x}(t_c^+[n+1]) = \mathbf{F}(\mathbf{x}(t_c^-[n+1])),$$

where $t_c[k]$ is the time of the kth collision, and t_c^- indicates just prior to the collision and t_c^+ is just after the collision. In order to estimate the gradients of the Poincare map, $\frac{d\mathbf{x}_p[n+1]}{d\mathbf{x}_p[n]}$, we must take a little care in handling the effects of initial conditions on the time (and therefore the state) of collision (using the chain rule). Linearizing about a trajectory $\mathbf{x}_0(t), \mathbf{x}_{p_0}[n]$ with impacts at $t_{c_0}[n]$, we have:

$$\frac{d\mathbf{x}_p[n+1]}{d\mathbf{x}_p[n]} = \left[\frac{\partial \mathbf{F}(\mathbf{x})}{\partial \mathbf{x}}\left[\frac{\partial \mathbf{x}(t)}{\partial \mathbf{x}_p[n]} + \mathbf{f}(\mathbf{x})\frac{dt_c[n+1]}{d\mathbf{x}_p[n]}\right]\right]_{t=t_{c_0}^-[n+1], \mathbf{x}=\mathbf{x}_0(t_{c_0}^-[n+1])}$$

The switching dynamics are defined by the zeros of scalar collision function, $\phi(t, \mathbf{x})$. Although these dynamics are time-varying in general (e.g., moving obstacles), for the rimless

[2] I hand it to SNOPT as a constraint.

wheel the collision function can be as simple as $\phi(\mathbf{x}) = \text{sgn}(\dot{\theta})(\theta - \gamma) - \alpha$. This collision function allows us to compute $\frac{dt_c[n+1]}{d\mathbf{x}_p[n]}$:

$$\frac{d\phi(t_c[n+1], \mathbf{x}(t_c^-[n+1]))}{d\mathbf{x}_p[n]} = 0 = \left[\frac{\partial \phi(t,\mathbf{x})}{\partial \mathbf{x}}\left[\frac{d\mathbf{x}(t)}{d\mathbf{x}_p[n]} + \frac{\partial \mathbf{x}(t)}{\partial t}\frac{dt_c[n+1]}{d\mathbf{x}_p[n]}\right] + \frac{\partial \phi(t,\mathbf{x})}{\partial t}\frac{dt_c[n+1]}{d\mathbf{x}_p[n]}\right]_{t=t_{c_0}^-[n+1], \mathbf{x}=\mathbf{x}(t_{c_0}^-[n+1])}$$

$$\frac{dt_c[n+1]}{d\mathbf{x}_p[n]} = -\left[\frac{\frac{\partial \phi(t,\mathbf{x})}{\partial \mathbf{x}}\frac{\partial \mathbf{x}(t)}{\partial \mathbf{x}_p[n]}}{\frac{\partial \phi(t,\mathbf{x})}{\partial t} + \frac{\partial \phi(t,\mathbf{x})}{\partial \mathbf{x}}\mathbf{f}(\mathbf{x})}\right]_{t=t_{c_0}^-[n+1], \mathbf{x}=\mathbf{x}(t_{c_0}^-[n+1])}$$

The final step, computing $\left[\frac{\partial \mathbf{x}(t)}{\partial \mathbf{x}_p[n]}\right]_{t=t_{c_0}^-[n+1]}$, can be done with a standard gradient calculation - see section 12.3.2 for the update.

EXAMPLE 5.3 Fixed points of the rimless wheel

Bifurcation diagram (as a function of slope) from computational search. Show that it agrees with analytical solution.

EXAMPLE 5.4 Fixed points of the compass gait

Bifurcation diagram (as a function of slope) - computational only.

5.7.2 Local Stability of Limit Cycle

In practice, the local stability analysis of a limit cycle is done by taking the derivatives around the fixed point of the return map. Again, this is often accomplished using numerical derivatives. Perturb the system in one direction at a time, evaluate the map and build the matrix ... From Goswami [37]. The eigenvalues of the derivative matrix of the Poincaré map, λ_i are called the *characteristic* or *Floquet* multipliers[83].

$$\mathbf{x}^* + \delta_1 = \mathbf{P}(\mathbf{x}^* + \delta_0) \approx \mathbf{P}(\mathbf{x}^*) + \left[\frac{\partial \mathbf{P}}{\partial \mathbf{x}}\right]_{\mathbf{x}^*} \delta_0.$$

$$\delta_1 \approx \left[\frac{\partial \mathbf{P}}{\partial \mathbf{x}}\right]_{\mathbf{x}^*} \delta_0.$$

A fixed point is stable if the $n-1$ non-trivial eigenvalues of this matrix are $|\lambda_i| < 1$.

Trivial multipliers vs. Non-trivial multipliers. Expect one *trivial* multiplier of 0, or 1 (which reveal the dynamics of a perturbation *along* the limit cycle orbit).

A standard numerical recipe for estimating $\frac{\partial \mathbf{P}}{\partial \mathbf{x}}$ is to perturb the system by a very small amount at least n times, once in each of the state variables, and watching the response. Be careful - your perturbation should be big enough to not get into integration errors, but small enough that it stays in the "linear regime". A good way to verify your results is to perturb the system in other directions, and other magnitudes, in an attempt to recover the same eigenvalues. In general, the matrix $\frac{\partial \mathbf{P}}{\partial \mathbf{x}}$ can be reconstructed from any

number of sampled trajectories by solving the equation

$$\begin{bmatrix} | & | & & | \\ \delta_1^1 & \delta_1^2 & \cdots & \delta_1^m \\ | & | & & | \end{bmatrix} = \left[\frac{\partial \mathbf{P}}{\partial \mathbf{x}}\right]_{\mathbf{x}^*} \begin{bmatrix} | & | & & | \\ \delta_0^1 & \delta_0^2 & \cdots & \delta_0^m \\ | & | & & | \end{bmatrix}$$

in a least-squares sense, where δ_0^i is the i-th perturbation (not a perturbation raised to a power!).

Lyapunov exponent. There is at least one quantifier of limit cycle (or trajectories, in general) stability that does not depend on the return map. Like a contraction mapping - perturb original trajectory in each direction, bound recovery by some exponential[83].

$$\|\delta(t)\| < \|\delta(0)e^{\mathbf{A}t}\|.$$

The eigenvalues of A are the Lyapunov exponents. Note that for a stable limit cycle, the largest Lyapunov exponent will be 1 (like the trivial floquet multiplier), and it is the remaining exponents that we will use to evaluate stability.

PROBLEMS

5.1. (CHALLENGE) *Closed-form solution for the rimless wheel.*

We have a closed-form expression for the return map, but can you find a solution for the entire return map dynamics? Given $\dot{\theta}[0]$, directly compute $\dot{\theta}[n]$ for any n. This would involve solving the quadratic difference equation.

5.2. (CHALLENGE) *Deadbeat control of the compass gait.*

Find a hip torque policy that produces a (locally) deadbeat controller.

6.832 Underactuated Robotics
Spring 2009